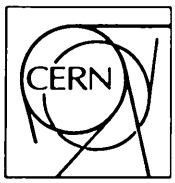

EUROPEAN ORGANIZATION FOR NUCLEAR RESEARCH

CERN - PS DIVISION

CERN/PS 2000-062 (OP)

A COMPARATIVE STUDY OF PROFILE AND SCRAPING METHODS FOR EMITTANCE MEASUREMENTS IN THE PS BOOSTER

C. Carli, A. Jansson, M. Lindroos, H. Schönauer

Abstract

It is important to have a clear understanding of the transverse emittance in a circular accelerator in order to achieve optimum brilliance. Experience with comparing emittance data from different instruments has shown that systematic errors can be important. In an attempt to detect such errors in the PS Booster, the emittance measurements are made according to two different principles: measurement of density distribution and measurement of amplitude distribution. In this paper we i) discuss these two principles and the theory behind them; ii) show how the data can be compared; iii) describe the instrumentation used for these measurements; and iv) present results for the typical PS Booster beams.

To be published in Particle Accelerators

Geneva, Switzerland
3 October 2000

A COMPARATIVE STUDY OF PROFILE AND SCRAPING METHODS FOR EMITTANCE MEASUREMENTS IN THE PS BOOSTER

C. CARLI, A. JANSSON, M. LINDROOS*, H. SCHÖNAUER

CERN, Geneva, Switzerland

It is important to have a clear understanding of the transverse emittance in a circular accelerator in order to achieve optimum brilliance. Experience with comparing emittance data from different instruments has shown that systematic errors can be important. In an attempt to detect such errors in the PS Booster, the emittance measurements are made according to two different principles: measurement of density distribution and measurement of amplitude distribution. In this paper we i) discuss these two principles and the theory behind them; ii) show how the data can be compared; iii) describe the instrumentation used for these measurements; and iv) present results for typical PS Booster beams.

KEY WORDS: Detectors, Instrumentation

1 INTRODUCTION

In an injector chain consisting of several accelerators and transfer lines, the emittance and the beam-optical parameters have to be known precisely to prevent transverse dilution at beam transfer. In day-to-day operation only the emittance is monitored, as any mismatch of optical parameters will result in an emittance increase. However, experience has shown that systematic errors associated with the instrument and the principle according to which it works make it difficult to compare emittance data, in particular from different machines. In an attempt to unveil systematic errors in the PS Booster instrumentation, the emittance measurements are made according to two different principles: measurement of density distribution ("profile") and measurement of amplitude distribution ("scraping")[1]. The amplitude distribution can be compared to the transverse profile data using an Abel transform.

* Corresponding Author. E-mail: Mats.Lindroos@cern.ch.

In this paper these two principles and the theory behind them are discussed. Furthermore, the instrumentation used for these measurements is presented together with some results for typical PS Booster beams.

2 MEASUREMENT OF AMPLITUDE DISTRIBUTION

2.1 Introduction

Scraping the circulating beam is a conceptually simple method to obtain the distribution of the betatron amplitudes $n(a)$ in a transverse plane. An aperture limitation is moved into the beam (or the beam is moved towards it) and the resulting relative beam loss is recorded. This can be done on consecutive machine cycles with different positions or by a fast-moving interceptor within a single cycle. One immediately obtains a set of values of the function

$$N(a) = \int_{-\infty}^{a} n(a')da' \tag{1}$$

if one knows the position of the beam centre, i.e. the closed orbit at the location of the aperture limitation. This is one of the practical difficulties of this approach, which is frequently circumvented by consecutive scraping from both sides to determine the centre. Numerical differentiation yields the wanted function $n(a)$. Measurements in a plane with finite dispersion yield a distribution which is a convolution of betatron amplitude and momentum distributions. In order to obtain the true betatron amplitude distribution, one needs to know the detailed momentum distribution for unfolding. The second moments, $\sigma_a^2 = \int a'^2 n(a')da'$ and $\sigma^2_{\text{scraped}}$ of the measured distribution, however, obey the simple law

$$\sigma^2_{\text{scraped}} = \sigma_a^2 + \sigma_p^2 \tag{2}$$

i.e., the calculation of σ_a^2 requires only the knowledge of the variance

$$\sigma_p^2 = D^2 \int (\Delta p/p)^2 n_p(\Delta p/p) d(\Delta p/p)$$

of the momentum dispersion. In order to obtain the projected density, one would need to apply an Abel type transform. However, the projected density itself is of little interest as it shows less detail and conveys less physical insight than the amplitude distribution. Thus it suffices to know the variance of the amplitude distribution to compare emittance measurements from a scraping method with those from a device measuring the projected density, which is simply

$$\sigma_\beta^2 = \sigma_a^2/2 \tag{3}$$

2.2 *Resolution of Scraping Methods*

All particles of a given betatron amplitude are located on a circle in normalised phase space. An intercepting obstacle, penetrating by an increment d per turn into this circle, cuts arc segments. At simple fractional tunes, corresponding to resonances like 1/2, 1/3, etc., these segments superpose exactly, and one realises immediately, that it takes many turns to scrape the whole circle away. This is of minor importance as the particles locked in low-order resonances would be unstable anyway. But even at irrational fractional tunes, complete scraping takes a certain number of turns, n_{scraped}, depending on the amplitude a and the increment d. A detailed account of the resolution limit and the following approximation for n_{scraped} can be found in Schönauer et al. [2], where it is shown that n_{scraped} can be written as

$$n_{\text{scraped}} = \frac{1}{2}\left(\frac{9\pi^2 a}{d}\right)^{1/3} \tag{4}$$

To give an example, for a target speed of 6 μm/turn, the particles of amplitude 5 mm appear smeared out over 0.125 mm or 2.5% of their amplitude. For beams of this size, scraping speeds of the order of $3-6\,\mu$m/turn are thus a good compromise between the duration of the measurement and its intrinsic accuracy limits.

2.3 *The BeamScope*

The full name behind the acronym, "BEtatron AMplitude Scraping by Closed-Orbit PErturbation"[3], describes the principle, illustrated in Fig. 1. A local orbit bump, produced by three pulsed dipoles, drives the beam progressively into a fixed aperture limitation, while the beam current and its numerically or electronically produced derivative are recorded by sampling-ADCs, together with the shunt signals of the bumper dipoles. The amplitude distribution can then be calculated. A typical output from the BeamScope in the PS Booster can be seen in Fig. 2.

For a machine like the PS Booster with its four rings, this was a more economic solution than moving an aperture limitation into the beam, since the (orbit correction) dipoles were already installed and only three multiplexed bumper power supplies were required. The price to pay is, however, an elaborate processing of the dipole signals in order to get the beam orbit position as precisely as possible. The processing includes, beyond the usual calibrations, a representation of the bench-measured magnetisation curves of the 24 correction dipoles involved, and a lattice code using the off-line measured and stored individual coherent tunes. Corrections for eddy current effects and electronic delays also have to be included.

The instrument displays the betatron amplitude distribution, the so-called 95% amplitude emittances and the emittance of the projected distribution. Projections are found by Abel transforms in the vertical plane and by polynomial fits in the horizontal plane, where the Abel transform is not directly applicable because of the effect of dispersion[4]. There is also the complication that the circumference of

the closed orbit due to the bump, which induces a counter-reaction from the radio frequency system that interferes with the measurement.

A crucial issue is the determination of the beam centre. Looking at the derivative of the recorded beam current, called the raw profile (see Fig. 3), the disappearance of this signal indicates that the beam centre has been scraped and all particles are lost. For the reasonable assumption of a locally uniform phase space density in the vicinity of the origin, the final slope of the derivative should theoretically be constant, with a sharp discontinuity at zero amplitude. The round-off and tails observed in reality stem from non-vanishing dispersion, limited electronic bandwidth and finite resolution. Putting a tangent on the turning point of the slope, its foot point represents the beams centre of a bunched beam even with finite dispersion and constitutes a good approximation for the other cases.

2.4 The "Beam Guillotine"

A fast mechanical scraper named "Beam Guillotine" has been built at TRIUMF for the PS Booster. This device will cross the aperture at speeds up to 10 m/s and will produce amplitude distributions directly, avoiding many of the complications of the BeamScope. The "Beam Guillotine" is scheduled for installation in spring 2000.

3 MEASUREMENT OF DENSITY DISTRIBUTION

3.1 Introduction

Several instruments measure the beam profile in real space, rather than the phase space particle density. These are instruments like secondary emission monitors, screens, wire-scanners and ionisation monitors. All these methods measure the density distribution, but differ widely in other respects, such as the spatial resolution.

The natural emittance definitions to use with these measurement methods are the σ-emittances, defined as

$$\epsilon_{x,1\sigma} = \frac{\sigma_\beta^2}{\beta_x} \tag{5}$$

and

$$\epsilon_{x,2\sigma} = \frac{4\sigma_\beta^2}{\beta_x}, \tag{6}$$

in terms of the standard deviation σ_β of the betatronic beam width and the optics parameter β_x. It might seem strange to have two definitions differing only by a fixed factor, but historically the 1σ emittance has been used for electron machines and the 2σ emittance for proton machines. The 2σ emittance is used in this paper.

The parameter which should be derived from the measured profile in order to deduce the emittance is the RMS beam width σ_{profile}. If the resolution of the measurement is high enough the discrete statistical formula

$$\sigma^2_{\text{profile}} = \left(\sum_i x_i^2 \rho_i \Big/ \sum_k \rho_k \right) - \left(\sum_j x_j \rho_j \Big/ \sum_k \rho_k \right)^2 \tag{7}$$

can be used. However, the profiles are often noisy, and even faint tails can falsify the result due to the high weight they are given in the formula. Therefore, additional data treatment is often necessary. This will involve suppression of the baseline and obviously erroneous data points, and/or the fitting of a curve to the data. One should bear in mind that it is very easy to falsify the results by using very elaborate fitting schemes, and the fitting should therefore be based on simple physical principles.

The most commonly used fit function is a Gaussian curve. A Gaussian fit reduces the N measured points to three or four parameters (mean position, width, baseline and maybe slope of baseline) and is therefore very over-constrained. This reduces the influence of noise on the profiles.

A spline interpolation on the other hand is under-constrained. For example, a cubic spline interpolation on N data points has $3N$ free parameters but only $3N - 4$ constraints. Thus, a spline fits any data set perfectly. It is therefore not useful for suppressing noise in the profiles. An approximate spline, where the perfect fit to the data points is traded for a small second derivative, is used for the PS Booster secondary emission monitors. The fitting routine has a free parameter which gives the relative weight between second derivative and the fit error. It has been found that the beam width, resulting from the fit, is very dependent on the parameter choice, especially in the case of narrow profiles.

An alternative way to get around the problem with noisy tails is to use Koziol's method[5], where the discrete statistical formula is applied only to the core of the distribution, and the truncated result is corrected assuming e.g. Gaussian tails. The core is defined as the part of the profile where the signal is larger than a certain threshold, which is a free parameter.

Whenever the discrete statistical formula is used, missing data points have to be accounted for. This can be done by replacing the missing point with an interpolation based on the surrounding points.

As in the case of scraping methods, the dispersive effects have to be accounted for. In the presence of dispersion, the physical beam profile is not only given by the betatron amplitude distribution, but has a contribution σ_p from the momentum spread of the beam. Thus,

$$\sigma^2_{\text{profile}} = \sigma^2_\beta + \sigma^2_p \tag{8}$$

where σ_p is the dispersive spread and σ_β is the pure betatronic width of the beam. The formula can easily be inverted to calculate the betatronic width from the

measured width, but obviously, if the dispersive term is large, it is important to measure it with the same accuracy as the beam width in order to get an accurate final result.

3.2 Wire Scanner

The fast wire scanner method for measuring beam profiles is based on the simple fact that an energetic particle beam traversing an obstacle, which in this case is a thin carbon wire, will cause secondary emission and a secondary particle shower, both proportional to the primary beam intensity at the wire location. The beam profile is either recorded by detecting the secondary particles or by measuring the secondary emission current as a function of the wire position. In a circular accelerator, such as the PS Booster, the wire is swept fast (> 10 m/s) through the circulating beam and consequently the recorded beam profile is the sum of all bunch profiles over many turns. Evidently, it is important that the closed orbit and the local Twiss β-value stays constant through the duration of the sweep. A detailed discussion of the fast wire scanners in low energy accelerators can be found in Elmfors et al.[6]. The main results are summarised here for convenience.

The geometry of the PS Booster wire scanners is shown in Fig. 4. The figure depicts an instant in the process of the wire sweeping through the beam. The mechanism consists of three parts: i) an electric motor with a crankshaft and a connecting rod, ii) a push- pull device connecting the motor via bellows to the fork inside the vacuum and iii) the U- shaped fork with the wire strung between the prongs. A decoder is connected to the motor, measuring its angular position from which the linear position of the wire is derived by geometrical considerations. The spatial resolution is much greater than that of secondary emission grids, due to a high sampling rate for the decoder (< 0.1 mm). The beam density can either be obtained through secondary emission from the wire (SE mode), or by observation of secondary particles with a scintillation detector (scintillator mode). Again, the baseline is determined and the variance extracted from the profile.

At very low energies, problems can be encountered is the scintillator mode as the secondary particles produced are few and have low energy. Since the detector is positioned outside the wire scanner vacuum chamber, low energy particles are stopped by the chamber wall. In Fig. 5 the total number of detected particles is plotted against energy. At approximately 150 MeV a sudden decrease in the number of particles can be observed. This corresponds to the threshold for pion production.

If the physical beam size is of the order of tens of millimetres, which is common in low-energy synchrotrons, several difficulties are encountered detecting the secondary particles. Firstly, the big change in angle between the detector and the wire during such a long sweep will falsify the deduced beam profile, as the secondary particle shower is highly anisotropic [6]. Secondly, at very large angles, the solid angle covered by the detector is so large as to cause deformation in the acquired profile.

A simple way of avoiding these geometrical problems is to use the SE mode rather than the scintillator mode. In Fig. 6 the profiles measured with a wire scanner at 50 MeV in the PS Booster with 4×10^{12} protons can be seen. The lower profile is from the scintillator and the upper one from the SE mode. The measurements were made on consecutive machine cycles. The asymmetry caused by the geometrical effects discussed above, in the case of secondary particle detection, is clearly visible.

Because of Coulomb scattering, the emittance of the beam will increase during the passage of the wire. To calculate this increase, the wire is pictured as a virtual foil, the thickness of which depends on the velocity and shape of the wire and the velocity of the beam. For the case of a wire with a circular cross section in a synchrotron with a revolution time of τ_0 (at $\beta_L = 1$) the virtual foil thickness (vft) can be written as

$$z_{\mathrm{vft}} = \frac{(2r)^2 \pi \beta_L}{4 v \tau_0} \quad . \tag{9}$$

Consequently, the emittance blow up due to the wire scanner device can be evaluated using the the well-known formula [7]

$$\epsilon = \epsilon_0 + \Delta\epsilon = \epsilon_0 + \frac{\pi}{2} \beta_T \langle \theta^2 \rangle. \tag{10}$$

Here ϵ_0 is the initial emittance and β_T the Twiss value at the wire scanner position. The RMS scattering angle will depend on the characteristics of the foil and the beam and is usually derived using formulas based on the Molière theory for multiple Coulomb scattering [8]. For small deflection angles, a good approximation for the RMS scattering angle is given by [9, 10]

$$\theta_0 = \frac{13.6 \text{ MeV}}{\beta p c} Q \sqrt{\frac{z}{X_0}} \left(1 + 0.038 \ln \left(\frac{z}{X_0} \right) \right), \tag{11}$$

where $p, \beta_L c$ and Q are momentum, velocity and charge number of the incident particles and $\frac{z}{X_0}$ is the thickness of the scattering medium in radiation lengths (z being the coordinate along the beam-line). However, the formula is only accurate to about 11% or better for $1 \times 10^{-3} < \frac{z}{X_0} < 100$. For a typical wire scanner with z_{vft} according to Eq. (9), $\frac{z_{\mathrm{vft}}}{X_0}$ is much smaller than 1×10^{-3}. The RMS scattering angle for a very thin wire, where the particles are scattered only once during the passage, can be estimated using the formula for Rutherford scattering. However, the case of the PS Booster wire scanner is intermediate. Calculating the RMS scattering angle using both approaches shows that the multiple scattering approach gives an upper limit. Typically in the PS booster at 50 MeV this upper limit is a few π mm mrad of emittance increase. This is to be compared to typically 100 π mm mrad of physical beam emittance at this energy. Above 300 MeV, the blow-up is insignificant compared to other sources of errors in the measurement.

3.3 Secondary Emission Monitors

Secondary Emission Monitors (SEM) are destructive or semi-destructive depending on the beam energy. They can either be made of thin ribbons (grid) or thin wires (harp). For emittance measurement purposes they are usually used in groups of three to provide three independent measurements of the beam width. The optimum positioning is such that the phase advance is 60° between the individual grids. The measured widths are related to the emittance by

$$\sigma_\beta = \sqrt{\epsilon\beta_i}, \qquad i = 1, 2, 3 \tag{12}$$

where the relations between the β_is can be derived from the transfer matrix T_{ij} between the grids, knowing that the Courant-Snyder invariant

$$A = \beta x'^2 + 2\alpha x x' + \gamma x^2 \tag{13}$$

is a conserved quantity. From these equations, the emittance and Twiss parameters can be derived. If the grids are separated only by drift spaces, the transfer matrix is unambiguously known, and one can expect a relatively high accuracy, limited only by the accuracy of the width measurement. In cases where magnets are present between the monitors, the error will increase due to the limited accuracy in the knowledge of the transfer matrix.

It should be stressed that any coupling between the transverse phase planes before, or in between the SEM-grids, will render this kind of measurement meaningless. Coupling introduces a correlation between the phase planes, which will make it impossible to extract the emittance from three width measurements.

The emittance can in principle be measured using only one SEM-grid or harp, if the preceding optics can be changed sufficiently in order to produce at least three independent width measurements.

If more than three harps are available, the extra data can be used either to make a χ^2-fit and get an error estimation, or to derive the additional parameters D, D' and $\Delta p/p$ directly from the profiles, instead of measuring them separately. This is, however, only possible if there is at least one bending magnet between the monitors[12]. The accuracy that can be expected in measuring the dispersion in this way is naturally lower than in a direct measurement when the beam energy is changed, but it can still be an interesting alternative, for example when the energy cannot be easily changed.

4 THE ABEL TRANSFORM

When one wishes to compare not only the emittances, obtained with scraping methods and profile measurements, but also the detailed shape of the distribution, one has to transform the amplitude distribution into a profile or vice versa. Details

are more clearly visible in amplitude distributions - profiles tend to be smoother than the underlying densities in phase space or oscillation amplitudes, and thus differences are more difficult to visualise.

To compare the shape of the distributions resulting from the two measurement methods, a profile has to be converted to an amplitude density by means of the Abel type integral transformation[13, 14]:

$$\rho(A) = -2\frac{d}{dA}\int_A^R d\eta \frac{g(\eta)\,\eta}{\sqrt{\eta^2 - A^2}} = -2A\int_A^R d\eta \frac{g'(\eta)}{\sqrt{\eta^2 - A^2}} \qquad (14)$$

where ρ means the density in normalised amplitudes $A = a/\sqrt{\beta}$ and g is the profile in normalised $\eta = x/\sqrt{\beta}$.

One should note, that Eq. (14) only applies if the measured profile is exclusively determined by the transverse betatron motion of the beam particles. If there is dispersion, which is usually not the case in the vertical plane, the profile is modified due to a contribution from the momentum spread and the above Abel type transform will not give a correct result[a].

5 MEASUREMENTS

The final emittances of the proton beams at CERN are determined by the multi-turn injection process in the PS Booster. As emittance control is of primordial importance for future LHC performance, the measurement of the emittances of the PS Booster beam, prior to ejection, requires an adequate accuracy and confidence in the measurement device. Confidence can only be established if comparisons of measurements can be made with different devices, preferably of different type, to avoid systematic shortcomings of a particular method. Their results should agree to the wanted accuracy, or differences should at least be explained in order to apply the appropriate corrections during data processing. Comparisons should extend over all the available range of beam emittances and intensities.

In the PS Booster, wire scanners have been chosen as the future main instrument for operational emittance measurements. A prototype wire scanner, installed for vertical measurements, has been compared with the existing BeamScope and, for measurement at ejection energy, with a triplet of SEM grids in the dedicated measurement line.

Measured emittances as a function of intensity at 1 GeV (PS Booster ejection energy in 1998) and at 200 MeV (roughly the lower limit for quantitative wire scanner measurements) are presented in Fig. 7 and Fig. 8, respectively. The general trend

[a] However, if the momentum distribution is known and uncorrelated with the transverse phase, one could still apply formula 14 to the profile after unfolding the contribution due to momentum width.

that wire scanner emittances are larger than those measured with BeamScope would be expected at 200 MeV, because the evaluation of the variance is extended over the whole wire scanner profile, which is asymmetric due to multiple scattering in the wire (cf. Fig. 9). This argument fails at 1 GeV (cf. Fig. 10), where the emittances obtained with the two instruments differ even more. Part, but certainly not all, of the difference could be explained by deviations of the local beta function from its theoretical value. In fact, such an error at the location of the BeamScope aperture restriction should be detected and compensated by the calibration procedure of the BeamScope[2].

Wire scanner measurements at 50 MeV, the injection energy of the PS Booster, should not be compared directly with BeamScope. Multiple scattering is so pronounced at this energy that there is considerable emittance blow-up during the passage of the wire. Particles that have gained large amplitudes will interact again when the wire moves out from the centre and will attain even larger amplitudes, until they eventually hit the walls. This loss is indeed observed and clearly visible in Fig. 11. This mechanism, by which the particles with a large amplitude are removed by the outgoing wire, explains that a subsequent BeamScope measurement on the same beam pulse will not "see" them and shows only a modest blow-up as in Table 2. Depending on the beam size and the scanning speed, there might even be an apparent emittance reduction after the wire has passed. The wire scanner however measures these particles before they are lost and thus records very large emittances. At this energy the very noisy and highly anisotropic scintillator signal, see Fig. 6, gives unreliable results.

Fig. 12 shows an interesting application of the wire scanner. It is very simple to track the normalised emittance through an acceleration cycle. It reveals a linear emittance blow-up of a high-intensity beam early in the acceleration, which does not occur at low intensities. A series of BeamScope measurements confirmed this fact.

5.1 Comparisons of Amplitude Distribution

The detailed shapes of the amplitude distribution, measured directly with the BeamScope and the one obtained applying an Abel type integral transform to a profile measured with a wire scanner, are compared in Fig. 9 and Fig. 10. Since the Twiss β function is not the same at the location of the two devices, the amplitudes (and positions of the profile) are given in normalised space, i.e. the amplitude divided by the square root of the β function is plotted rather than the amplitude.

The measured data points of the profile are smoothed applying a Savitzky-Golay filter (of order 3, taking typically 20 to 40 points on either side) and then interpolated by a spline of order 3.

Since the Abel assumes rotational symmetry in normalised phase space, the profile should ideally be symmetric around the beam centre. In reality, the two half-profiles

are slightly different. Both half-profiles can be introduced into Eq. (14), giving two approximations of the amplitude distributions.

The limits of the half-profile are defined by the beam centre and the closest point at which the signal has fallen below a certain threshold.

One of the reasons why the profile is not exactly symmetric, is scattering in the wire. The leading edge of the profile, which is passed first, is not yet affected by the scattering and thus generally steeper, resulting in a steeper fall-off of the amplitude density. The amplitude distribution computed with the second half-profile has a fall-off which is less sharp than the one of the original distribution.

In Fig. 9 amplitude densities are compared at 200 MeV. The profile obtained applying the Abel type transform to the first half profile (solid curve with the steeper fall-off) agrees well with the BeamScope measurement (dashed curve). Both vary significantly from a Gaussian, plotted as a dot-dashed line for comparison. It is typical for the PS Booster that the amplitude distribution is close to constant in the centre of the beam and falls off rapidly at the edge. If the Abel transform is applied to the second half-profile (solid curve with flatter fall-off) scattering systematically alters the result.

In Fig. 10 the amplitude densities obtained from a wire scanner profile measurement via the Abel transform is compared with the direct measurement by the BeamScope for a beam of 1 GeV. At higher energies the blow-up and the smoothing of the profile due to scattering is less important. Thus it is not surprising that the amplitude distribution obtained with the second half-profile also agrees well with the BeamScope result.

6 CONCLUSIONS

Although the BeamScope and the wire scanner agree well for small LHC-type beams, where confidence in the measurements is most important, the differences for larger emittances raises doubts. At the time of writing, there is no convincing explanation for the observed systematic divergence, which makes it difficult to determine which of the two devices gives the more accurate result. The SEM grid results equally plotted in Fig. 7 are not trustworthy. Due to the large step of the grid, the applied spline fit turns out to be strongly dependent on the fitting parameters. In fact, a subsequent comparison study revealed that a Gaussian fit yields better results, despite the fact that the real betatron amplitude distribution is far from Gaussian (see Fig. 10).

With the installation of wire scanners in the PS Booster, the emittance in the LHC injector chain can be measured in all machines, including the LINAC, using profile methods, which allows direct comparisons. The role of the scraping methods will be detailed studies of e.g. amplitude distributions, in particular at the lowest energies and calibration of the profile devices. The SEM-grids in the PS Booster

measurement line will be replaced by SEM-harps with smaller wire spacing. This should allow reliable profile measurements even for the small emittance LHC beam. The use of wire scanners in lower energy machines, like the PS Booster, is new. This has been made possible by the mechanical improvements of the instrument, the use of multi-fibre carbon wires and careful calibration of the wire movement. The use of the SE-current for signal detection has proved superior, providing better signal quality and less dependence on secondary particle shower anisotropy.

ACKNOWLEDGEMENTS

We would like to thank all our colleagues at the PS Division for their support, in particular C. Carter, H. Koziol, J-M. Nonglaton, J. Olsfors and U. Raich.

REFERENCES

1. M.Arruat, C.Carli, H.Koziol, M.Lindroos, J.Olsfors, U.Raich, H.Schönauer, "A Comparative Study of Fast Wire Scanners, BeamScope and SEM-Grids for Emittance Measurements at the PS Booster", Proc. 3rd DIPAC, Frascati (Rome), p. 129, 1997
2. H. Schönauer, "Beamscope: Physics considerations, implementation and results of tests", CERN internal note: CERN/PS/BR/82-2
3. H.Schönauer, "Beamscope - a Novel Device for Measuring Emittances and Betatron Amplitude Distributions", IEEE Trans. Nucl.Sci. NS-26, p. 3294, 1979
4. M.Martini, H.Schönauer, "Methods to Compare and to Obtain Representative Emittance Values from Fundamentally Different Measurement Devices", Proc. 1st DIPAC, Montreux, p. 146, 1993.
5. H.Koziol, "Evaluation of Near-Gaussian Distributions with Ill-Defined Tails", Note: LAMPF, MP-3-74-1
6. P.Elmfors, A.Fasso, M.Huhtinen, M.Lindroos, J.Olsfors and U.Raich, "Wire Scanners in Low Energy Accelerators", Nucl. Instr. and Meth. **A396** (1997) 13-22
7. P. J. Bryant, "Beam transfer lines" in: Proceedings of the CERN Accelerator school, Fifth general accelerator physics course, Editor: S. Turner, Jyväskylä, Finland, 1992.
8. H. A. Bethe, Phys. Rev. **89**, 1256 (1953).
9. V. L. Highland, Nucl. Instr. and Meth. **129**, 497 (1979).
10. G.R. Lynch and O.I. Dahl, Nucl. Instr. and Meth. **B58**, 6 (1991).
11. P.L.Walden, "Meson Production Reactions by p, d, ? ... on Nuclei", Nuclear Physics A 374, p.277, 1982.
12. G.Arduini, M.Giovannozzi, D.Manglunki, M.Martini, "Multigrid Measurements in a Transfer Line", CERN internal note: CERN/PS/DI/Note 98-03
13. P.W. Krempl, "The Abel-type Integral Transformation with the Kernel $(t^2 - x^2)^{-1/2}$ and its Application to Density Distributions of Particle Beams", CERN internal note: CERN - Note MPS/Int. BR/74-1
14. C. Carli, M. Lindroos and H. Schönauer, "Comparision of Amplitude Profiles from BeamScope and Wire Scanner Measurements for the Vertical Plane in the PSB", CERN internal note: PS/CA Note 99-11

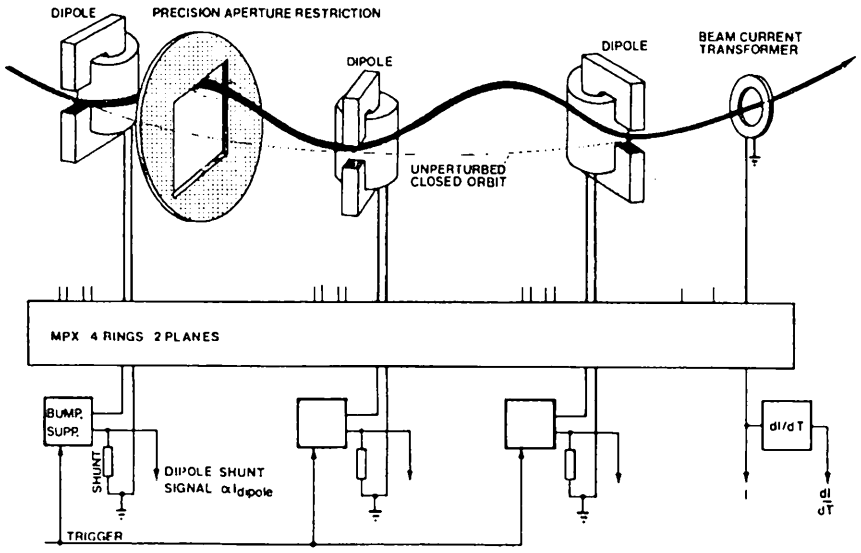

FIGURE 1: Artists view of the BeamScope.

Ring	ϵ_h	ϵ_v	ϵ_{h_n}	ϵ_{v_n}	ϵ_{hp}	ϵ_{vp}	ϵ_{hp_n}	ϵ_{vp_n}	IP[E 10
1	10.2	7.4	18.5	13.4	4.6	4.5	8.3	8.1	126.8
2	12.6	7.0	22.9	12.7	6.5	4.5	11.8	8.1	126.0
3	12.2	8.9	22.0	16.2	6.9	5.2	12.5	9.4	120.7
4	13.4	7.2	24.2	13.0	7.7	4.9	14.0	8.8	156.2

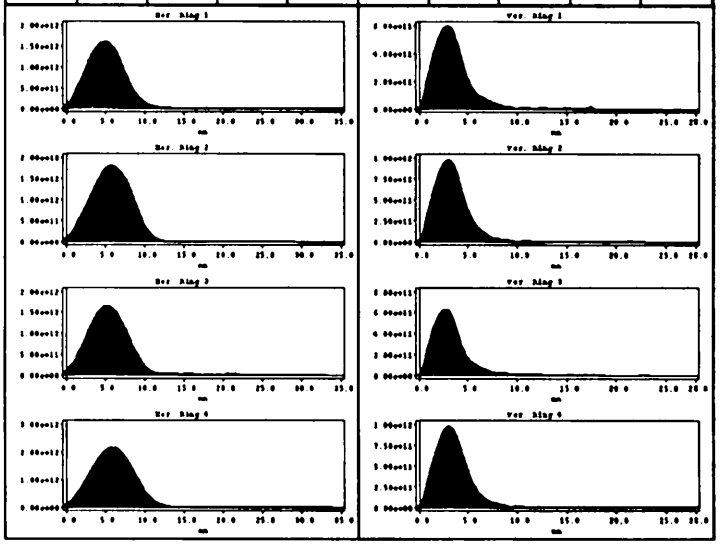

FIGURE 2: BeamScope Measurements on an LHC-type beam in all four PS Booster rings. $\epsilon_{h,v}$ denote the emittances encompassing 95% of the initially circulating particles, subscript p the 2σ emittances of the projected profiles, n indicates normalised values.

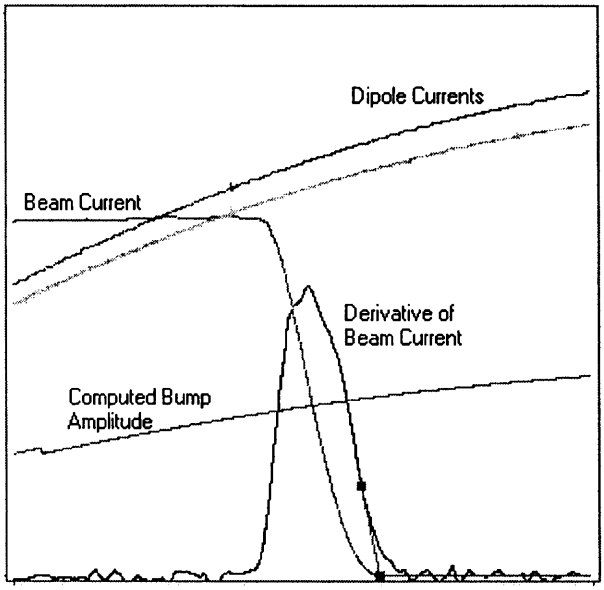

FIGURE 3: The five raw signals used by BeamScope: the shunt signals from the three bumper dipoles (two of them are equal and appear as a single trace), the beam current and its electronically produced derivative. Also displayed is the computed bump amplitude. Its discontinuity indicates the numerical delay applied to this signal to compensate for the real delay due to eddy currents in the vacuum chamber. One may also notice the noise on the raw signals. While the high-frequency component can be easily smoothed out, the lower frequency perturbations of the derivative present a problem and can compromise the tangent fit, which is always shown for verification. The horizontal axis spans 6 ms and the vertical one 1024 bits, or 102.4 mm for the computed bump.

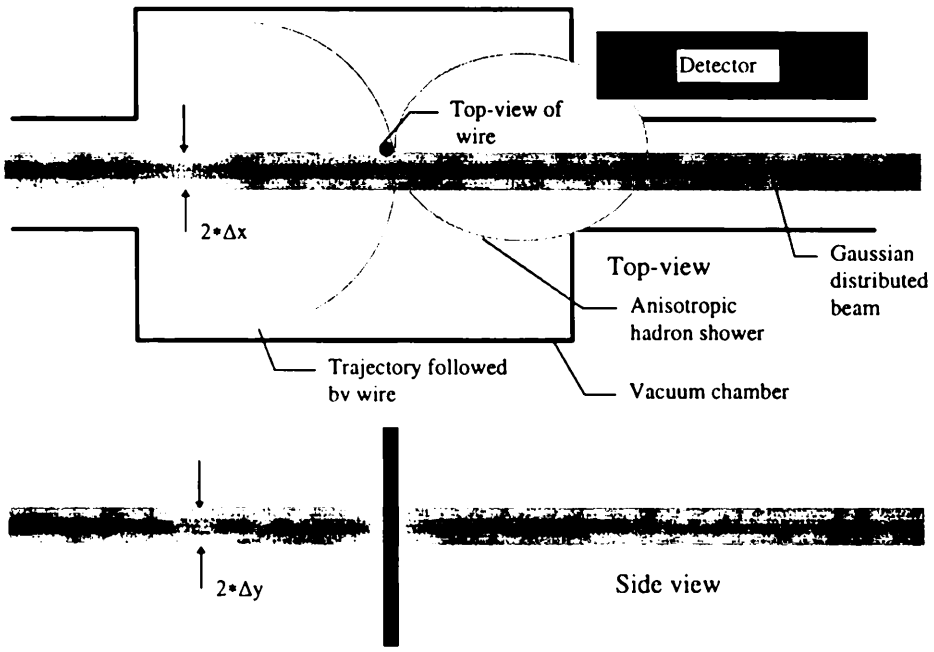

FIGURE 4: Geometry of beam and wire for a horizontal measurement ($\Delta x = 1\sigma_x$ and $\Delta y = \sigma_y$).

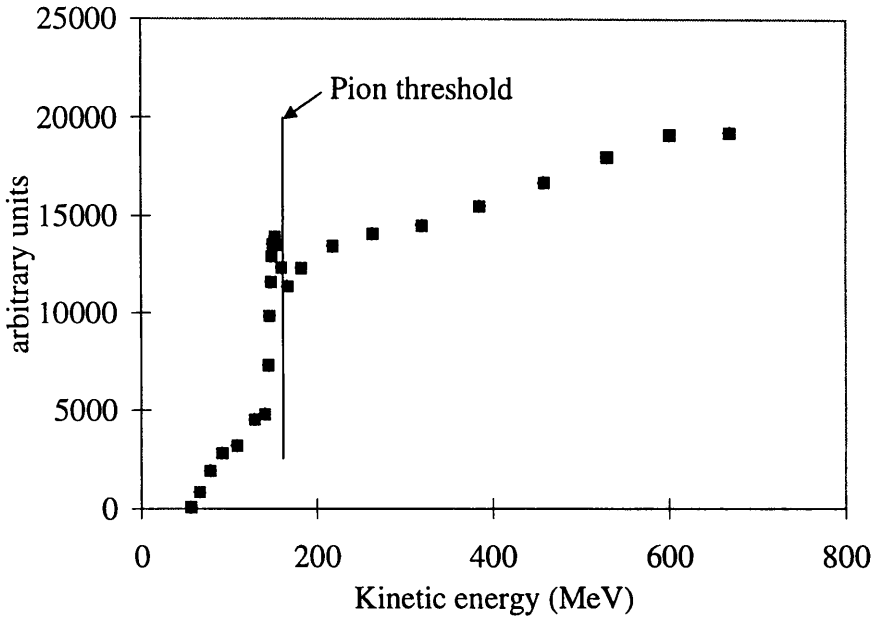

FIGURE 5: Integral over profile for constant photo-multiplier voltage, as a function of the beam energy. At 150 MeV the pion threshold is clearly visible. The peak in intensity just above this threshold is probably due to nuclear effects, see e.g. Walden[11]. All measurements were made with 5×10^{11} protons.

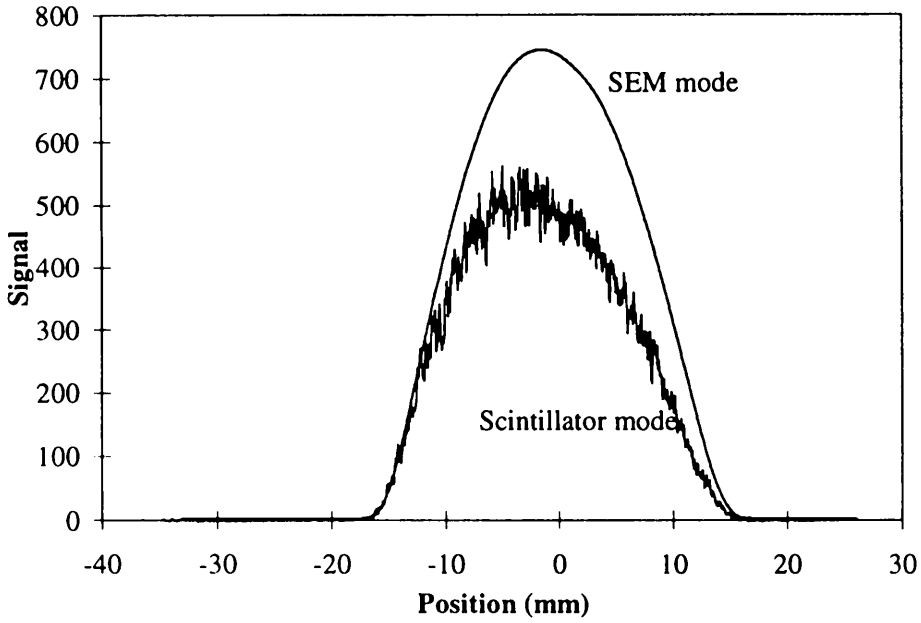

FIGURE 6: Profiles measured with the wire scanner at 50 MeV in the PS Booster with 4×10^{12} protons. The lower profile is from the scintillator signal and the upper one from the secondary electron emission. The measurements were made on consecutive machine cycles. It has been shown [6] that the asymmetry in the lower profile is mainly due to the asymmetric secondary particle shower combined with geometric effects in the detector-wire set-up. The contribution from multiple scattering is small compared to these effects.

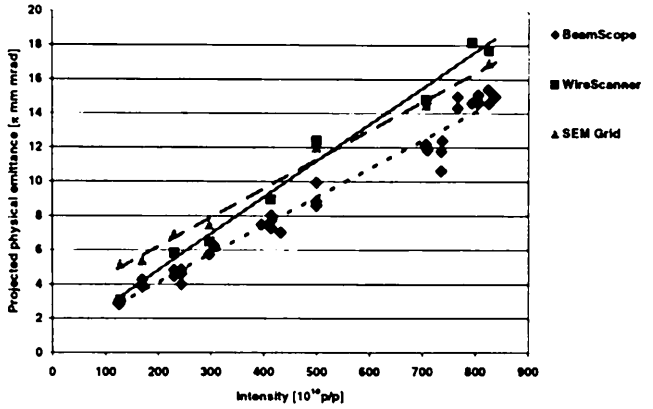

FIGURE 7: Emittance as a function of intensity at 1 GeV measured with the BeamScope, the Wire scanner and the SEM-grid.

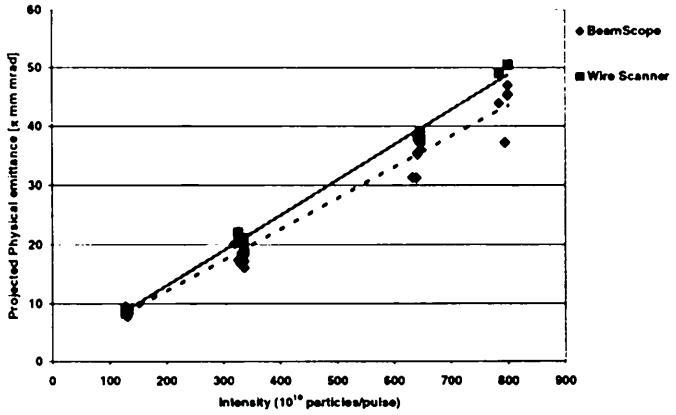

FIGURE 8: Emittance as a function of intensity at 200 MeV measured with the BeamScope and the Wire scanner.

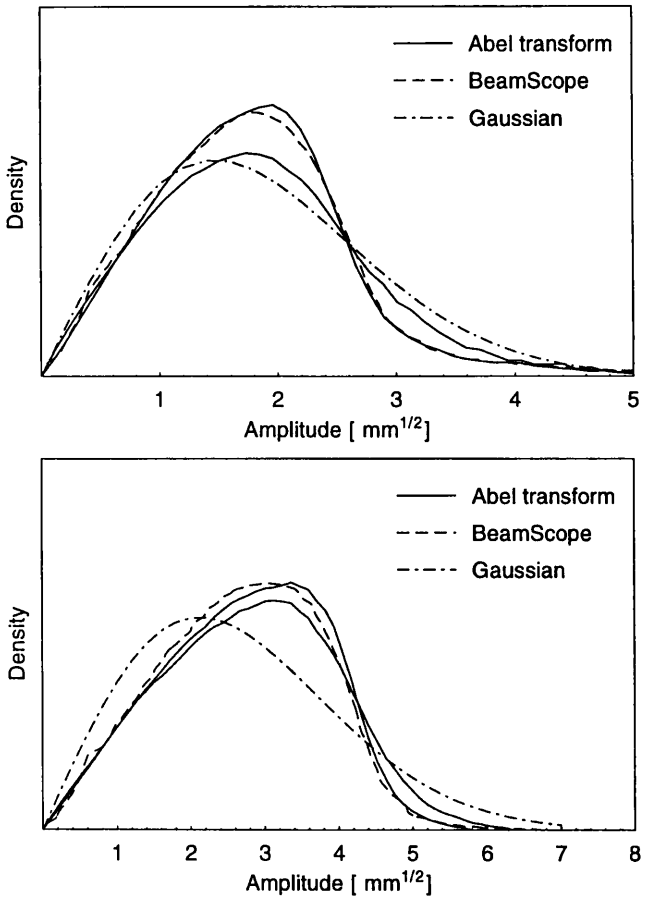

FIGURE 9: Comparisons of amplitude densities at a 200 MeV flat top. The solid lines are obtained from the wire scanner measurements via an Abel type transform using the two different half-profiles. The dashed lines are directly measured with the BeamScope. The dash-dot line shows the amplitude density for a Gaussian beam of approximately the same emittance. The upper figure is for a low intensity beam and the lower figure for a high intensity beam.

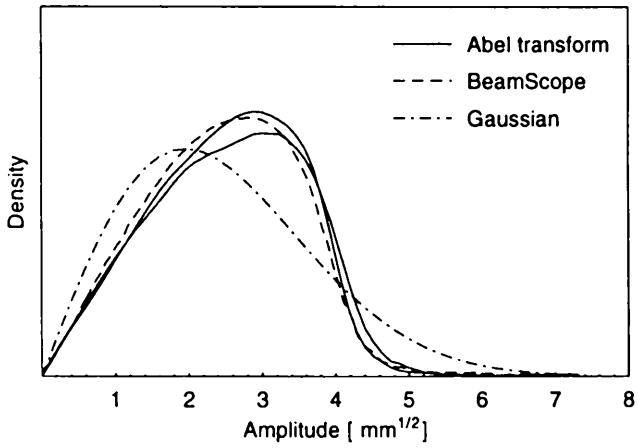

FIGURE 10: Comparison of amplitude densities at a 1 GeV flat top.

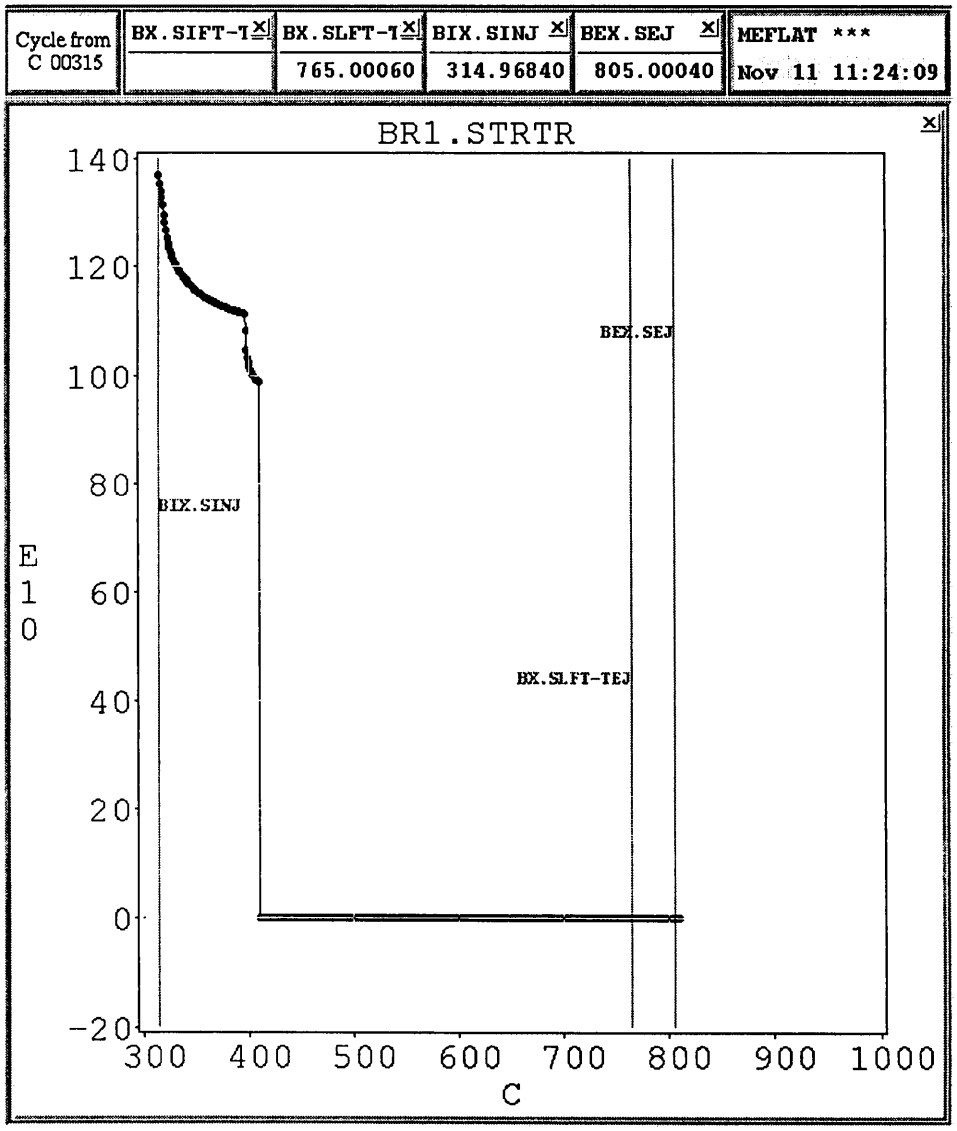

FIGURE 11: Display of a beam current transformer signal, involving a wire scanner measurement ($\epsilon = 42.4\ \pi\, mm\, mrad$) followed by a BeamScope measurement ($\epsilon = 32.2\ \pi\, mm\, mrad$) at 50 MeV. On the x-axis the time is in units of ms, starting at a reference point in the cycle and on the y-axis the intensity in units of 10^{10} protons/pulse. Observe that the wire scanner measurement at 400 ms induces losses at 50 MeV. The subsequent BeamScope measurement at 415 ms is inherently destructive.

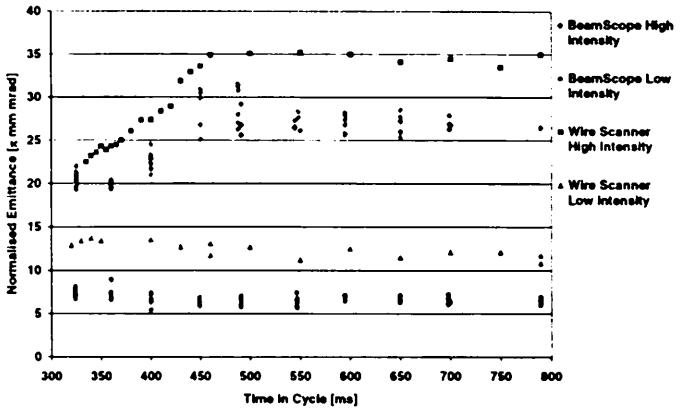

FIGURE 12: Emittance as a function of energy, at low and high intensity, measured with the BeamScope and the Wire scanner.

TABLE 1: Definitions of greek and roman symbols used in this paper

Symbol	Description	Definition
β_L	Relativistic β Lorentz factor	
γ_L	Relativistic γ Lorentz factor	
β	Lattice (Twiss) parameter	
α	Lattice (Twiss) parameter	
γ	Lattice (Twiss) parameter	
ϵ	Physical 2σ emittance	$(2\sigma)^2/\beta$
ϵ^*	Normalised 2σ emittance	$\beta_L\gamma_L\epsilon$
σ_β	Standard deviation of projected betatron distribution	
σ_a^2	Second moment of amplitude distribution	
σ_p	Dispersion contribution to the beam width	$D\delta p/p$
σ_{profile}	Standard deviation of measured projected beam	
$\sigma^2_{\text{scraped}}$	Second moment of measured amplitude distribution	
ρ_i	Transverse beam distribution function at data point i	
θ	Average scattering angle	
c	velocity of light	
D	Transverse dispersion function	
n_p	Density function in $\delta p/p$	
$\delta p/p$	1σ momentum spread	
τ_0	Revolution time at $\beta_L = 0$	
Q	Charge state	
x_i	Physical position corresponding to data point i	
X_0	Radiation length	
z_{vft}	Equivalent foil thickness of a wire sweeping through the beam	

TABLE 2: Measurements of the projected physical beam emittance at 50 MeV with the BeamScope and the Wire scanner. The BeamScope measurement was either done on the next beam pulse or the same beam pulse. In the case that the measurements were done in the same pulse the BeamScope measurement was done after the wire scanner measurement. All the emittances in units of π mm mrad.

Wire scanner:		**BeamScope:**	
SEM signal	Scintillator signal	In next pulse	In the same pulse
42.9		27	
42.3		26	
42.4			32.2
41.1		26.7	
	38.7	26.2	
	40.8	26.3	
	37.6		28.4
	40.1		31.9